Analyzing the effect of ion binding to the membrane-surface on regulating the light-induced transthylakoid electric potential ($\Delta\Psi_m$)

Hui Lyu [1]* and Dušan Lazár [2]*

[1]School of Biological Science and Agriculture, Qiannan Normal University for Nationalities, Duyun, China, [2]Department of Biophysics, Faculty of Science, Palacký University, Olomouc, Czechia

The transthylakoid membrane potential ($\Delta\Psi_m$) is essential because it can drive the ATP synthesis through the CF_0-CF_1 type of ATP-synthase in chloroplasts as an energetic equivalent similar to ΔpH. In addition, a high fraction of proton motive force (PMF) stored as the $\Delta\Psi_m$ component is physiologically important in the acclimation of photosynthesis to environmental stresses. It has been shown that $\Delta\Psi_m$ is the sum of the Donnan potential difference ($\Delta\Psi_{dn}$) and the diffusion potential difference ($\Delta\Psi_d$). Specifically, $\Delta\Psi_{dn}$, $\Delta\Psi_d$, and $\Delta\Psi_m$ are strongly associated with the ionic activities near the membrane surface, particularly, the extent of ion binding to the charged/neutral sites adjacent to the membrane surface. However, an in-depth analysis of the effect of altered cationic binding to the membrane surface on adjusting the transthylakoid electric potentials ($\Delta\Psi_{dn}$, $\Delta\Psi_d$, and $\Delta\Psi_m$) is still missing. This lack of a mechanistic understanding is due to the experimental difficulty of closely observing cations binding to the membrane surface *in vivo*. In this work, a computer model was proposed to investigate the transthylakoid electric phenomena in the chloroplast focusing on the interaction between cations and the negative charges close to the membrane surface. By employing the model, we simulated the membrane potential and consequently, the measured ECS traces, proxing the $\Delta\Psi_m$, were well described by the computing results on continuous illumination followed by a dark-adapted period. Moreover, the computing data clarified the components of transthylakoid membrane potential, unraveled the functional consequences of altered cationic attachment to the membrane surface on adjusting the transthylakoid electric potential, and further revealed the key role played by Donnan potential in regulating the energization of the thylakoid membrane. The current model for calculating electric potentials can function as a preliminary network for the further development into a more detailed theoretical model by which multiple important variables involved in photosynthesis can be explored.

KEYWORDS

ions, thylakoid membrane, Donnan potential, diffusion potential, membrane potential, mathematical model

Introduction

Light-driven electron transport triggers the proton translocation across thylakoid membranes, because of which, a transmembrane proton motive force (PMF) is established. Transmembrane proton motive force consists of two components, i.e., a chemical (expressed as ΔpH) and an electrical component (expressed as $\Delta\Psi_m$), which is defined by:

$$\text{PMF} = \Delta\Psi_{m,i-o} \left(\frac{2.3\text{RT}}{\text{F}}\right) \Delta\text{pH}_{\text{o-i}} \qquad (1)$$
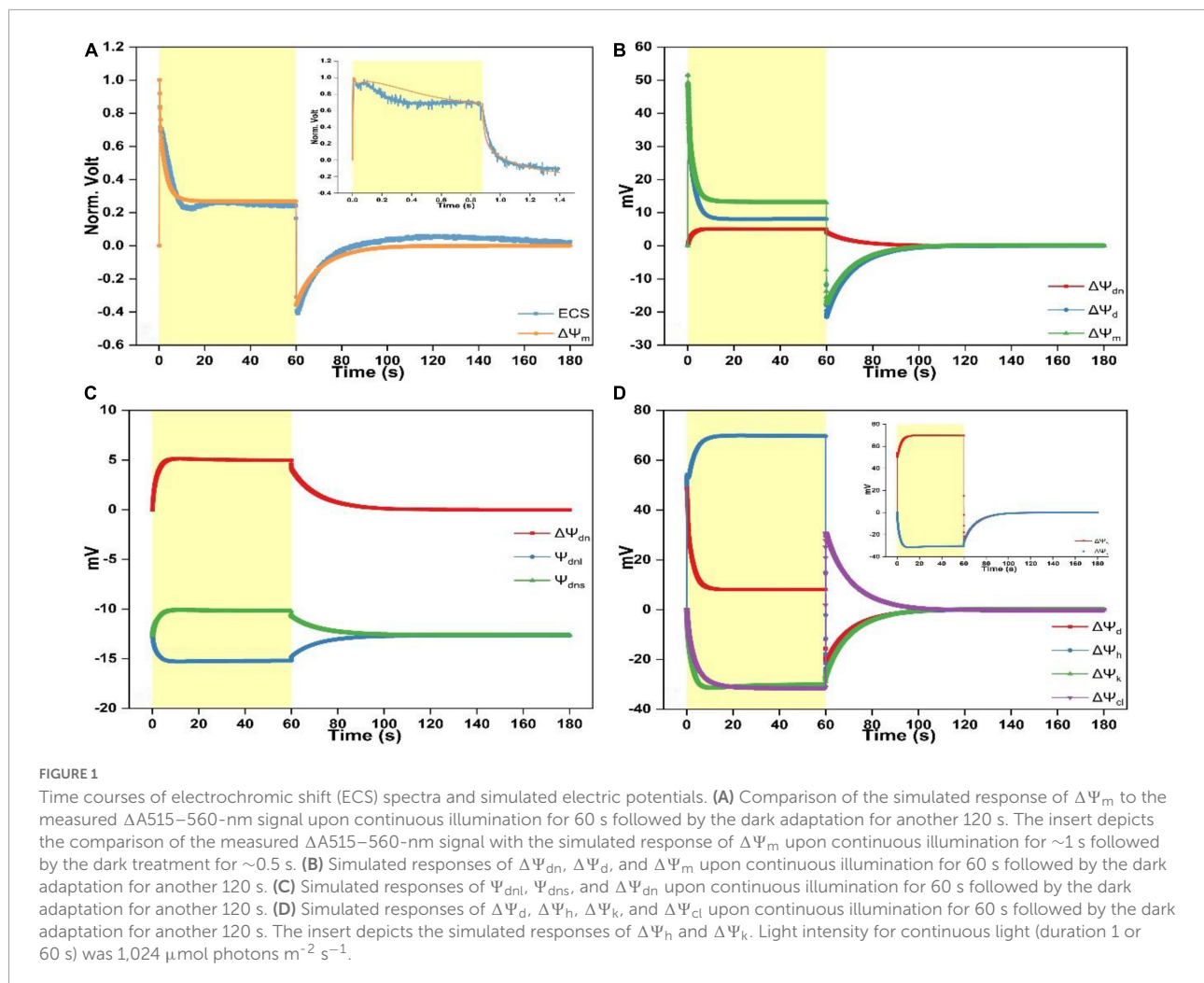
where $\Delta\Psi_{m,i-o}$ and ΔpH_{o-i} represent the electric potential difference and the pH difference across thylakoid membranes, respectively. They are calculated as outside (stroma) minus inside (lumen) for ΔpH and inside (lumen) minus outside (stroma) for $\Delta\Psi_m$. The variables R, T, and F are the universal gas constant, the absolute temperature, and the Faraday constant, respectively. The PMF is the driving force for ATP synthesis facilitated by the CF_0–CF_1 type of ATP-synthase in chloroplasts. The two components of PMF are thermodynamically equivalent to drive ATP formation according to the chemiosmotic hypothesis (Mitchell, 1961, 1966, 2011). The ratio of PMF parsing into $\Delta\Psi_m$ and ΔpH is a crucial quantity for reconciling the light use efficiency under rapid changes in environmental conditions (Davis et al., 2016, 2017; Li et al., 2021). More importantly, strong lumen acidification can initiate the process of non-photochemical quenching (NPQ) to protect photosystem II (PSII) from over-excitation by converting the excess light energy into heat (Li et al., 2009; Pinnola and Bassi, 2018). On the other hand, $\Delta\Psi_m$ is physiologically essential because it not only functions to promote the ATP yield but also serves to regulate the electron transport reaction by affecting the midpoint redox potentials of electron acceptors and electron donors (Bulychev, 1984; Vredenberg and Bulychev, 2003; Davis et al., 2016). In addition, a high fraction of PMF stored as the

---

Abbreviations: ATP, adenosine triphosphate; PMF, proton motive force; NPQ, non-photochemical quenching; PSII, photosystem II; ΔpH, transthylakoid pH difference; $\Delta\Psi_m$, membrane potential difference; $\Delta\Psi_{dn}$, Donnan potential difference; Ψ_{dn}, Donnan potential; Ψ_{dnl}, luminal Donnan potential; Ψ_{dns}, stromal Donnan potential; $\Delta\Psi_d$, diffusion potential difference; $\Delta\Psi_h$, electric potential difference caused by H^+ translocation; $\Delta\Psi_k$, electric potential difference caused by K^+ translocation; $\Delta\Psi_{Cl}$, electric potential difference caused by Cl^- translocation; K_{cmgl}/K_{cmgs}, binding constant of Mg^{2+} attached to negative charge site on luminal/stromal membrane surface; K_{pmgl}/K_{pmgs}, binding constant of Mg^{2+} attached to neutral site on luminal/stromal membrane surface; K_{pkl}/K_{pks}, binding constant of K^+ attached to neutral site on luminal/stromal membrane surface; K_{phl}/K_{phs}, binding constant of H^+ attached to neutral site on luminal/stromal membrane-surface; $[SC]_l$ $([SC]_s)$, density of negative charge site on luminal (stromal) membrane surface; $[SP]_l$ $([SP]_s)$, density of neutral site on luminal (stromal) membrane surface; d_s, thickness of membrane surface charge layer; κ, Debye–Hückel parameter; ECS, electrochromic shift; GHK, Goldman–Hodgkin–Katz; TSRT, transition state rate theory; ρ, density of non-neutralized membrane-fixed negative charge; qE, energy-dependent NPQ of chlorophyll fluorescence; OEC, oxygen evolving complex.

$\Delta\Psi_m$ component is particularly important during transitions from high to low light (Wang and Shikanai, 2019; Basso et al., 2020; Correa Galvis et al., 2020).

Moreover, $\Delta\Psi_m$ is responsive to many factors including the composition of the bathing solution, the activity of proton pumping, the state of ion channels/transporters, and ionic activities near the membrane surface, which are themselves responsive to $\Delta\Psi_m$ (Kinraide et al., 1998). It has been shown that $\Delta\Psi_m$ is the sum of the Donnan potential difference ($\Delta\Psi_{dn}$) and the diffusion potential difference ($\Delta\Psi_d$) (Ohshima and Ohki, 1985; Ohshima and Kondo, 1987, 1988a,b, 1990). Specifically, Ψ_{dn} is the consequence of the interaction between solute ions in the contacting bulk-phase and the fixed charges arising from the protein ligands, since the thylakoid membrane is the lipo-protein system which carries the negative charges mainly due to carboxyl groups (probably glutamic and aspartic acid residues) of exposed segments of integral membrane protein constitutes (Barber, 1980b, 1982). The specific value of the negative charges may be determined based on the microelectrophoresis studies and varies in terms of the plant species and physiological conditions within the same breed (Nakatani et al., 1978). The electrostatic $\Delta\Psi_{dn}$ is often sufficiently negative to attract mobile divalent cations (e.g., Mg^{2+}) more than mobile monovalent cations (e.g., K^+, H^+) and repel the mobile anions (e.g., Cl^-, OH^-). Previously, Siggel proposed a preliminary model to probe the role played by $\Delta\Psi_{dn}$ during photosynthesis in a series of works (Siggel, 1981a,b,c). To date, the common neglect of $\Delta\Psi_{dn}$ in a range of photosynthetic simulations probably reflects the computational complexity when all heterogeneous ions *in situ* together with the cations binding to the membrane surface are taken into account. Nevertheless, the existence of $\Delta\Psi_{dn}$-induced electrical phenomena near the thylakoid membrane should be considered for an improved understanding of many aspects of the photosynthetic events in and around the thylakoid membrane (Barber, 1980b, 1982; Kaňa and Govindjee, 2016). An alternative approach to theoretically analyze the ion charge interaction adjacent to the membrane surface, termed the Gouy–Chapman double-layer potential, assumes that the thickness of membrane surface charge layer (d_s) is zero and all membrane fixed charges are only located within the membrane surface (Barber, 1980a; Ohshima and Ohki, 1985; Ohshima and Kondo, 1990). This hypothesis may be unjustified because for a usual biological membrane, the d_s is commonly non-zero (Levine et al., 1983). Under this circumstance, the electrical potential in the region far inside the charge layer is practically equal to the Donnan potential (Ohshima and Kondo, 1988b).

The diffusion potential difference ($\Delta\Psi_d$) is initiated by the light-induced electron-coupled proton translocation which causes the luminal acidification. This eventually triggers the proton efflux through the ATP-synthase and the transthylakoid ion movement *via* ion channels/transporters.

FIGURE 1

Time courses of electrochromic shift (ECS) spectra and simulated electric potentials. **(A)** Comparison of the simulated response of $\Delta\Psi_m$ to the measured $\Delta A515-560$-nm signal upon continuous illumination for 60 s followed by the dark adaptation for another 120 s. The insert depicts the comparison of the measured $\Delta A515-560$-nm signal with the simulated response of $\Delta\Psi_m$ upon continuous illumination for ~1 s followed by the dark treatment for ~0.5 s. **(B)** Simulated responses of $\Delta\Psi_{dn}$, $\Delta\Psi_d$, and $\Delta\Psi_m$ upon continuous illumination for 60 s followed by the dark adaptation for another 120 s. **(C)** Simulated responses of Ψ_{dnl}, Ψ_{dns}, and $\Delta\Psi_{dn}$ upon continuous illumination for 60 s followed by the dark adaptation for another 120 s. **(D)** Simulated responses of $\Delta\Psi_d$, $\Delta\Psi_h$, $\Delta\Psi_k$, and $\Delta\Psi_{cl}$ upon continuous illumination for 60 s followed by the dark adaptation for another 120 s. The insert depicts the simulated responses of $\Delta\Psi_h$ and $\Delta\Psi_k$. Light intensity for continuous light (duration 1 or 60 s) was 1,024 µmol photons m^{-2} s^{-1}.

Early electrophysiological experiments showed that thylakoid-harbored cation pores are permeable to K$^+$ and Mg^{2+} (Pottosin and Schönknecht, 1996), while anion pores are permeable to Cl$^-$ (Schönknecht et al., 1988). The recent molecular biological assays confirmed the existence of K$^+$/H$^+$ antiporter KEA3 (Kunz et al., 2014; Basso et al., 2020), the voltage-gated Cl$^-$ channel VCCN1 (Herdean et al., 2016b), and the Cl$^-$ channel CLCe (Herdean et al., 2016a). The co-function of the proton translocation and the channel/transporter mediated ion movement ultimately determine the $\Delta\Psi_d$ which itself conversely impact the redistribution of ions and homeostasis of the stacked membranous system.

Numerous studies have concentrated majorly on the interrelationship between the chemical component of PMF (ΔpH) and its impact on photosynthetic processes. However, less effort was put on explorations of the electric component of PMF. Here, we proposed a photosynthetic model, which is an extension of a previously published version (Lyu and Lazar, 2017a,b), to determine the effect of ion attached to the thylakoid membrane surface on regulating $\Delta\Psi_{dn}$, $\Delta\Psi_d$,

and $\Delta\Psi_m$. Toward this end, the extension of model includes the determination of Ψ_{dn} and the corresponding change of quantities induced by Ψ_{dn}. Taken together, our goal was to gain a mechanistic insight into these variations in the highly complex and dynamic network of photosynthetic processes.

Materials and methods

Measurements were conducted with 10-day tobacco leaves (*Nicotiana tabacum*), grown in a growth chamber at 20°C on artificial soil composed of Perlit and Knop's solution. The light regime was 8 h dark/16 h light (continuous white irradiation of 90 µmol photons m^{-2} s^{-1}). Measured P515 signal was used as a proxy for $\Delta\Psi_m$ (Klughammer et al., 2013). The P515 ($\Delta A515-550$ nm) signal reflects the electrochromic shift (ECS) of absorption maximum of pigments (chlorophylls and carotenoids), which is proportional to $\Delta\Psi_m$ across the thylakoid membrane (Witt, 1979; Vredenberg, 1981; Joliot and Joliot, 1989). ECS and P515 are used as synonyms in the text. The

P515 signal measurements were done using Dual-PAM-100 system (Heinz Walz GmbH, Effeltrich, Germany) equipped with the P515/535 module. The system measures transmittance at 515 and 550 nm, and then their difference is assessed. The P515 signal was detected during continuous illumination of adaxial leaf side by white light of high intensity (1,024 μmol photons m^{-2} s^{-1}). The measurements have been accomplished with seven different leaves and the typical curves are shown in **Figure 1A** and its inset. All samples were dark-adapted for 10 min before measurements.

Description of the model

A comprehensive model of proton-coupled electron transport in and around photosynthetic thylakoid membranes has been proposed in our previous studies (Lyu and Lazar, 2017a,b). The model was made up of several modules including the linear and cyclic electron transport, the proton outflow through ATP-synthase, Calvin-Benson cycle and regulatory pathways. Moreover, the ion fluxes were calculated based on the modified Goldman–Hodgkin–Katz (GHK) equation (Van Kooten et al., 1986) and/or the transition state rate theory (TSRT) (Lyu and Lazar, 2017b). All quantitative values for model parameters are taken from literature and details of the model are given in our previous studies (Lyu and Lazar, 2017a,b). In the previous model, the ion–charge interaction was roughly speculated based on a preliminary calculation for the surface potential. In this work, we introduce the Donnan equilibrium potential to elaborate on the electrical phenomena adjacent to the thylakoid membrane-surface. Overall, Ψ_{dn} can regulate the distribution of ions close to the membrane surface causing the enrichment of cations and repulsion of anions; hence, adjusting the dynamics of channels/antiporters mediated ion fluxes and the proton efflux through ATP-synthase.

To clarify, the overall concept of the model is presented in **Scheme 1**. The onset of the electron transport is coupled to the proton translocation from the stroma into the lumen. The PMF is thus established and then consumed to drive the ATP synthesis through the CF_0–CF_1 type of ATP-synthase in chloroplasts. The early electrophoresis findings show that the negative charge density (~ -0.035 C/m^2) on the luminal side is higher than on the stromal side (~ -0.025 C/m^2) (Barber, 1982). Nonetheless, to equilibrate the initial transthylakoid Donnan potential in darkness, the fixed negative charge on either membrane surface is evenly assigned the value of -0.035 C/m^2 (Barber, 1982). Several early physiological measurements also showed a rise, upon illumination, of Mg^{2+} concentration in the stroma by 1–5 mM (Krause, 1977; Portis, 1981) and it was speculated that the change of stromal Mg^{2+} concentration may affect the thylakoid stacking and hence the efficiency of energy transfer between photosystems I and II (Barber et al., 1977), but the relative contribution of Mg^{2+}

ions remains a matter of discussion because Tester and Blatt (1989) also reported that there was no Mg^{2+} current in a direct measurement of ion movement by fusing spinach thylakoid vesicles into planar lipid bilayers (Tester and Blatt, 1989). It seems that the Mg^{2+} flux presented in the literature vary greatly and is highly impacted by assay conditions. Therefore, it has been suggested that the Mg^{2+} flux may only play a small part in balancing the light-driven H$^+$ movements (Tester and Blatt, 1989) and it has also been suggested that under physiological conditions the current through the cation selective channel is mainly carried by K$^+$ ions (Pottosin and Schönknecht, 1996). Furthermore, the Mg^{2+} related channels/antiporters in thylakoid membranes have not been identified so far by modern molecular studies. Therefore, it would be reasonable to only consider K$^+$ and Cl$^-$ as the main ions penetrating the membrane to modify the electric potentials, which has been suggested as well in a recently published model to *in silico* study the partitioning of PMF upon various light conditions (Li et al., 2021). To follow up, ions of K$^+$ and Cl$^-$ are redistributed to partition $\Delta\Psi_m$ into $\Delta\Psi_d$ and $\Delta\Psi_{dn}$ *via* ion channels/antiporters, namely, the voltage-gated K$^+$ channel V–K$^+$, the K$^+$/H$^+$ antiporter KEA3, the voltage-gated Cl$^-$ channel VCCN1, and the Cl$^-$ channel CLCe. The resultant effect of ion redistribution causes the formation of the diffusion potential difference ($\Delta\Psi_d$) which consists of three components, i.e., $\Delta\Psi_h$, $\Delta\Psi_k$, and $\Delta\Psi_{cl}$. The concepts and terms necessary for the understanding of the results and discussion are described below and detailed description of all computational segments of the model is provided in **Supplementary Material**.
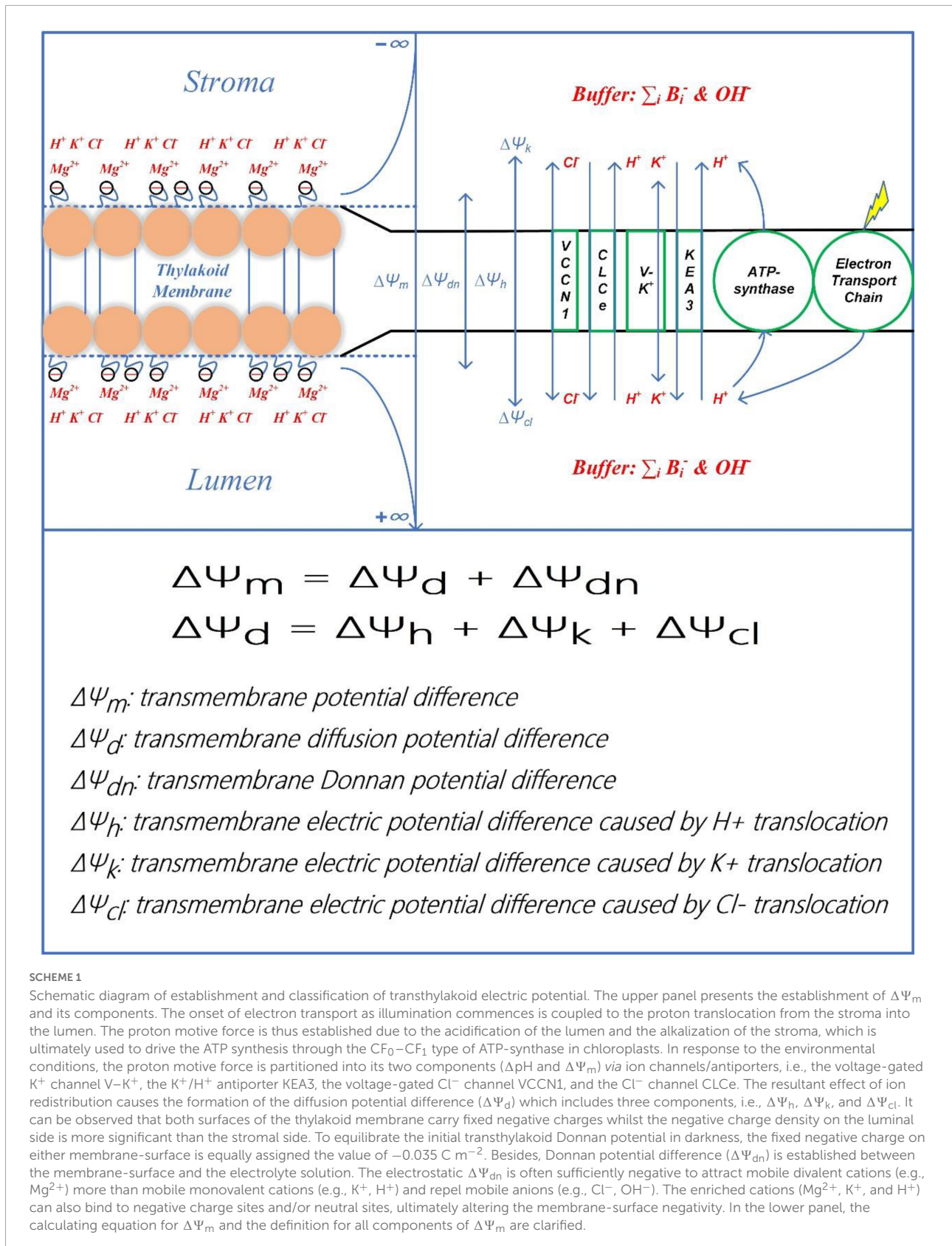
The calculation of electrical potential difference

As presented above, $\Delta\Psi_m$ is responsive to the composition of the contacting solution, the activity of proton pumping, the state of ion channels/antiporters, and electrical characteristics near the membrane surface. In brief, $\Delta\Psi_m$ and $\Delta\Psi_d$ can be calculated by (see **Scheme 1**):

$$\Delta\Psi_m = \Delta\Psi_d + \Delta\Psi_{dn} \qquad (2)$$

$$\Delta\Psi_d = \Delta\Psi_h + \Delta\Psi_k + \Delta\Psi_{cl} \qquad (3)$$

Where $\Delta\Psi_m$ equals to the sum of $\Delta\Psi_d$ and $\Delta\Psi_{dn}$; $\Delta\Psi_h$, $\Delta\Psi_k$, and $\Delta\Psi_{cl}$ sum up to form $\Delta\Psi_d$; $\Delta\Psi_d$, $\Delta\Psi_{dn}$, $\Delta\Psi_h$, $\Delta\Psi_k$, and $\Delta\Psi_{cl}$ are caused, respectively, by the light-induced transmembrane redistribution of bulk electrolytes, by the interplay of negative thylakoid-membrane surface charges and the bathing solute ions, by the transmembrane H$^+$ movement and H$^+$ released from oxygen evolving complex (OEC), by the transmembrane K$^+$ movement, and by the transmembrane Cl$^-$ movement. More information on calculation of $\Delta\Psi_d$ can be obtained in our previous works (Lyu and Lazar, 2017a,b).

SCHEME 1

Schematic diagram of establishment and classification of transthylakoid electric potential. The upper panel presents the establishment of $\Delta\Psi_m$ and its components. The onset of electron transport as illumination commences is coupled to the proton translocation from the stroma into the lumen. The proton motive force is thus established due to the acidification of the lumen and the alkalization of the stroma, which is ultimately used to drive the ATP synthesis through the CF_0-CF_1 type of ATP-synthase in chloroplasts. In response to the environmental conditions, the proton motive force is partitioned into its two components (ΔpH and $\Delta\Psi_m$) *via* ion channels/antiporters, i.e., the voltage-gated K^+ channel V$-K^+$, the K^+/H^+ antiporter KEA3, the voltage-gated Cl^- channel VCCN1, and the Cl^- channel CLCe. The resultant effect of ion redistribution causes the formation of the diffusion potential difference ($\Delta\Psi_d$) which includes three components, i.e., $\Delta\Psi_h$, $\Delta\Psi_k$, and $\Delta\Psi_{cl}$. It can be observed that both surfaces of the thylakoid membrane carry fixed negative charges whilst the negative charge density on the luminal side is more significant than the stromal side. To equilibrate the initial transthylakoid Donnan potential in darkness, the fixed negative charge on either membrane-surface is equally assigned the value of -0.035 C m^{-2}. Besides, Donnan potential difference ($\Delta\Psi_{dn}$) is established between the membrane-surface and the electrolyte solution. The electrostatic $\Delta\Psi_{dn}$ is often sufficiently negative to attract mobile divalent cations (e.g., Mg^{2+}) more than mobile monovalent cations (e.g., K^+, H^+) and repel mobile anions (e.g., Cl^-, OH^-). The enriched cations (Mg^{2+}, K^+, and H^+) can also bind to negative charge sites and/or neutral sites, ultimately altering the membrane-surface negativity. In the lower panel, the calculating equation for $\Delta\Psi_m$ and the definition for all components of $\Delta\Psi_m$ are clarified.
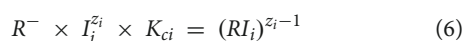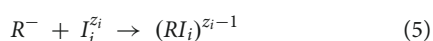
The Donnan potential determination involving the ion attachment to the membrane surface

The Donnan potential is the electrical potential at which the electroneutrality of the entire system is reached (Ohshima and Kondo, 1990). It occurs due to the excess of impermeant anions (e.g., charged macromolecules and/or organic acids) sequestered in a living cell. This nonzero potential changes the concentrations of solute ions near the membrane away from their values in the bulk solution (Gillespie and Eisenberg, 2001), which can be determined from:
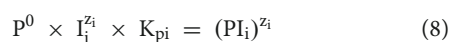
$$\sum_{i=1}^{N} z_i C_i^{\infty} \exp\left(-\frac{z_i F \Psi_{dn}}{RT}\right) + \frac{\rho}{F} \times ro = 0 \qquad (4)$$

where z_i is the valence of the ith ion ($i = 1, 2, \ldots, N$), C_i^{∞} is the bulk concentration of the ith ion, F is the Faraday constant, R is the universal gas constant, T is the absolute temperature, ρ is the density of the non-neutralized membrane-fixed negative charges, and ro is the ratio of surface-area to volume, which is assigned the value of 10^6 cm^{-1} for thylakoid (Van Kooten et al., 1986).

Ions binding to the membrane-surface are incorporated by altering ρ in Eq. (4). Here, ρ depends in part on intrinsic surface charge density and also includes those solute ions that bind to the membrane surface. In this study, the model takes into account 1:1 binding of cations to a negatively charged site ([R$^-$]) and a neutral site ([P^0]) as described in the following reactions:

$$R^- + I_i^{z_i} \rightarrow (RI_i)^{z_i-1} \qquad (5)$$

$$R^- \times I_i^{z_i} \times K_{ci} = (RI_i)^{z_i-1} \qquad (6)$$

and

$$P^0 + I_i^{z_i} \rightarrow (PI_i)^{z_i} \qquad (7)$$

$$P^0 \times I_i^{z_i} \times K_{pi} = (PI_i)^{z_i} \qquad (8)$$

and

$$I_i^{z_i} = C_i \times \exp\left(-\frac{z_i F \Psi_{dn}}{RT}\right) \qquad (9)$$

Thus, ρ can be computed from Eqs (4) to (8) as follows:

$$\frac{\rho}{F} \times ro = -\left[R^-\right] + \sum_{i=1}^{N} (z_i-1) + \left[(RI_i)^{z_i-1}\right]$$

$$+ \sum_{i=1}^{N} z_i \left[(PI_i)^{z_i}\right] \qquad (10)$$

where z_i is the valence of the ith ion ($i = 1, 2, \ldots, N$), I_i^{zi} is the Ψ_{dn}-induced concentration of the ith ion close to the membrane surface, [R$^-$] and [P^0] denote concentrations

of the negatively charged sites and the neutral sites ([R$^-$] equals to 3.63×10^{-5} mol/cm^3 reflects [SC] which was set at -0.035 C/m^2; P^0 reflects [SP] and was assigned 8-fold of [R$^-$]), [(RI$_i$)$^{z_i-1}$] and [(PI$_i$)^{zi}] denote product concentrations of the ith ion binding to the negatively charged site and the neutral site. For cations binding to the negative charge sites, both divalent (Mg^{2+}) and monovalent species (K$^+$ and H$^+$) are considered in simulations. However, it can be observed from Eq. (10) that the concentration of negative charges remains unaffected provided a neutralized pair is randomly created for the monovalent cations binding to the negative charges. These formulas were initially proposed to investigate the rhizotoxicity of heavy metals binding to the root cell membrane (Kinraide et al., 1998). Unless stated otherwise, all theoretical details and parameter values involved in the formulations are presented in **Supplementary Material**.

Results

Following continuous illumination for 60 s and the ensuing 120 s in darkness, the ECS kinetics is in accordance with the previously reported measurements (Kramer and Sacksteder, 1998; Johnson and Ruban, 2014). Specifically, upon switching on the light, the ECS kinetics shows a sharp rise before decaying to ~30% of its initial amplitude and then rising again till saturating within ~20 s. When the light is switched off, the ECS signal shows a sharp fall before returning to the steady-state a bit higher above the dark baseline (**Figure 1A**). Overall, the ECS kinetics was well described by the modeled $\Delta\Psi_m$ whereas the simulation lacks the shallow dip positioned during ~10 to ~30 s, and the ECS kinetics as illumination ceases appears to relax a bit faster than the modeled curve. According to Johnson and Ruban (2014), the transient dip and the following changes leading to the steady-state before illumination ceases is the slow phase of ECS, which is not caused by $\Delta\Psi_m$ but the formation of qE-related absorption change. However, Kramer et al. suggested that a significant fraction of PMF in chloroplasts can be stored as $\Delta\Psi_m$ under the steady-state conditions (Kramer and Sacksteder, 1998; Kramer et al., 1999; Cruz et al., 2001, 2005; Davis et al., 2017; Kanazawa et al., 2017). Our simulations show that the lasting ECS trace is partly contributed by $\Delta\Psi_{dn}$ (see **Figure 1B**), and the dip may be related to K$^+$ redistribution induced by the alteration of abundance of membrane surface charges on luminal surface or both surfaces ([SC]$_l$ or [SC]$_l$ and [SC]$_s$) (see **Figures 2E,F**). The insert of **Figure 1A** shows the comparison between the modeled $\Delta\Psi_m$ and the ECS signal upon illumination for ~1 s followed by a 0.5-s period of darkness. The measured ECS curve shows a bimodal pattern as illumination commences before decaying to a plateau. Upon switching off the light, the curve shows an exponential decay till reaching a steady-level largely below the dark baseline, in line with the measurements previously reported in the literature (Bulychev, 1984; Vredenberg, 1997;
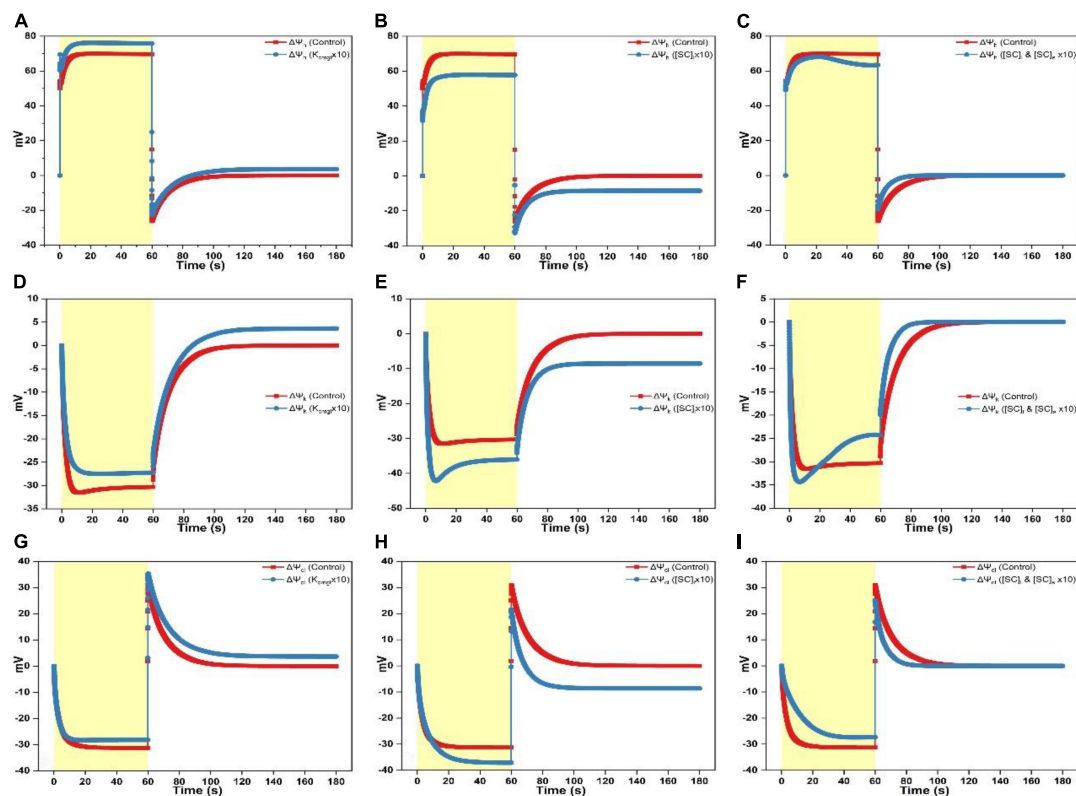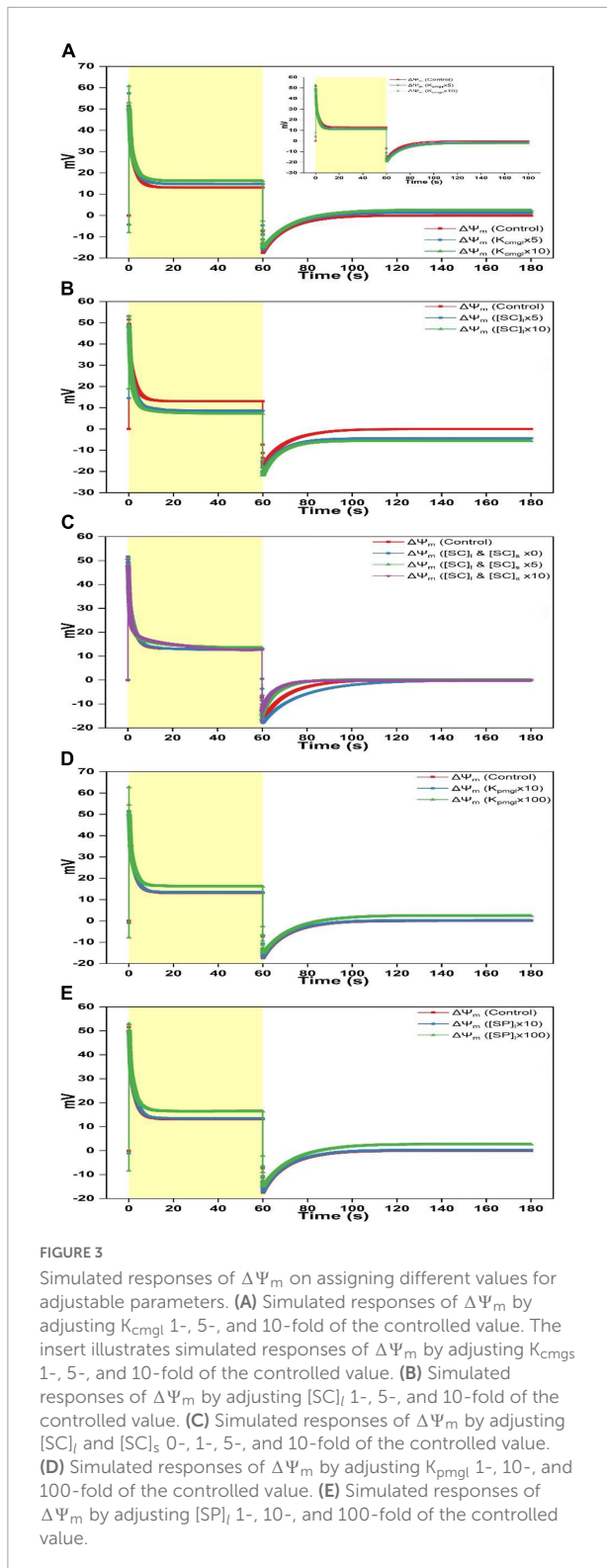
FIGURE 2

Simulated responses of $\Delta\Psi_h$, $\Delta\Psi_k$, and $\Delta\Psi_{cl}$ on assigning different values for adjustable parameters. **(A)** Simulated responses of $\Delta\Psi_h$ by adjusting K_{cmgl} 1- and 10-fold of the controlled value. **(B)** Simulated responses of $\Delta\Psi_h$ by adjusting $[SC]_l$ 1- and 10-fold of the controlled value. **(C)** Simulated responses of $\Delta\Psi_h$ by adjusting $[SC]_l$ and $[SC]_s$ 1- and 10-fold of the controlled value. **(D)** Simulated responses of $\Delta\Psi_k$ by adjusting K_{cmgl} 1- and 10-fold of the controlled value. **(E)** Simulated responses of $\Delta\Psi_k$ by adjusting $[SC]_l$ 1- and 10-fold of the controlled value. **(F)** Simulated responses of $\Delta\Psi_k$ by adjusting $[SC]_l$ and $[SC]_s$ 1- and 10-fold of the controlled value. **(G)** Simulated responses of $\Delta\Psi_{cl}$ by adjusting K_{cmgl} 1- and 10-fold of the controlled value. **(H)** Simulated responses of $\Delta\Psi_{cl}$ by adjusting $[SC]_l$ 1- and 10-fold of the controlled value. **(I)** Simulated responses of $\Delta\Psi_{cl}$ by adjusting $[SC]_l$ and $[SC]_s$ 1- and 10-fold of the controlled value.

Bulychev and Vredenberg, 1999). The modeled $\Delta\Psi_m$ can reproduce several features of the measured curve, e.g., the bimodal pattern, the timing of the first peak and the transient dip after the first peak, and the decaying kinetics in the darkness. However, the second peak of simulation appears to be less prominent than in the ECS signal, which may be related to the proton translocation induced by the alteration of abundance of membrane-surface charges on both membrane sides ($[SC]_l$ and $[SC]_s$) (see **Figure 2C**). **Figure 1B** shows that $\Delta\Psi_{dn}$ and $\Delta\Psi_d$ sum up to form $\Delta\Psi_m$ in which ~40% amplitude of the steady-state $\Delta\Psi_m$ is contributed by the formation of $\Delta\Psi_{dn}$ (~5 mV). The simulated $\Delta\Psi_{dn}$, which is the difference of Ψ_{dns} minus Ψ_{dnl}, is shown in **Figure 1C**. The negativity of Ψ_{dnl} is increased because of the light-driven cation efflux into the stroma (K^+ out and H^+ out) and anion influx into the lumen (Cl^- in). The Donnan equilibrium potential in either compartment is usually less than ~ -20 mV (Sperelakis, 2012) and apparently our results are approaching to this value.

The separation of the simulated $\Delta\Psi_d$ into three components, namely, the electric potential difference caused by

H^+ translocation ($\Delta\Psi_h$), by K^+ translocation ($\Delta\Psi_k$), and by Cl^- translocation ($\Delta\Psi_{cl}$) is shown in **Figure 1D**. As the light is switched on, the $\Delta\Psi_h$ trace shows a sharp rise followed by a dip before rising again till reaching a steady-state. In contrast, $\Delta\Psi_k$ and $\Delta\Psi_{cl}$, as the counterpart of $\Delta\Psi_h$, both decreased although $\Delta\Psi_k$ decreased initially faster than $\Delta\Psi_{cl}$ till reaching a negative steady-level (**Figure 1D**). As the light is switched off, the $\Delta\Psi_h$ trace contains a sharp fall till the inverted $\Delta\Psi_h$ attains the negative maximum and then followed by a slow relaxation returning to the dark baseline which is attributable to the leaky proton influx into the lumen (**Supplementary Figures 3A,B**). The inverted $\Delta\Psi_h$ would suddenly force Cl^- back into the stroma till $\Delta\Psi_{cl}$ is inverted to the positive maximum before relaxing to the dark baseline (**Figure 1D**). Simultaneously, the K^+ flux out of the lumen will be decelerated due to the inverted $\Delta\Psi_h$ till $\Delta\Psi_k$ converges to the dark baseline. Notably, the $\Delta\Psi_k$ relaxing trace during the dark phase is overlapped by the $\Delta\Psi_h$ trace (insert of **Figure 1D**). This is understandable since the K^+ efflux is mediated by the V–K^+ channel which is strictly voltage dependent.

FIGURE 3

Simulated responses of $\Delta\Psi_m$ on assigning different values for adjustable parameters. **(A)** Simulated responses of $\Delta\Psi_m$ by adjusting K_{cmgl} 1-, 5-, and 10-fold of the controlled value. The insert illustrates simulated responses of $\Delta\Psi_m$ by adjusting K_{cmgs} 1-, 5-, and 10-fold of the controlled value. **(B)** Simulated responses of $\Delta\Psi_m$ by adjusting $[SC]_l$ 1-, 5-, and 10-fold of the controlled value. **(C)** Simulated responses of $\Delta\Psi_m$ by adjusting $[SC]_l$ and $[SC]_s$ 0-, 1-, 5-, and 10-fold of the controlled value. **(D)** Simulated responses of $\Delta\Psi_m$ by adjusting K_{pmgl} 1-, 10-, and 100-fold of the controlled value. **(E)** Simulated responses of $\Delta\Psi_m$ by adjusting $[SP]_l$ 1-, 10-, and 100-fold of the controlled value.

To investigate the effect of ion attached to the membrane surface on regulating $\Delta\Psi_{dn}$, $\Delta\Psi_d$, and $\Delta\Psi_m$, the controlling parameters that affect electric characteristics close to the membrane surface are adjusted including the binding constant

of Mg^{2+} attached to the negative charge sites on both surfaces (K_{cmgl} and K_{cmgs}), the binding constants of Mg^{2+}, K^+, and H^+ attached to the neutral sites on both surfaces (K_{pmgl}, K_{pmgs}, K_{pkl}, K_{pks}, K_{phl}, and K_{phs}), the density of the negative charge site on both surfaces ($[SC]_l$ and $[SC]_s$), and the density of the neutral site on both surfaces ($[SP]_l$ and $[SP]_s$). The change of these parameters or their compositions can take place near the luminal surface or the stromal surface or both. Since the variation of parameters near the stromal surface leads to the kinetics, which is sorted in a reverse order in comparison to the variation on single luminal surface (e.g., see insert of **Figure 3A**). Here, we consider the change of parameters occurring only on luminal surface or both surfaces. On luminal side, we have conducted simulations for 36 times by adjusting $[SC]_l$ (control, 5-, and 10-fold), $[SP]_l$ (0-fold, control, 10-, and 100-fold, the same change for the parameter composition followed), K_{cmgl}, K_{pmgl}, K_{pkl}, K_{phl}, $[K_{pmgl}K_{pkl}]$, $[K_{pmgl}K_{phl}]$, $[K_{pkl}K_{phl}]$, and $[K_{pmgl}K_{pkl}K_{phl}]$, respectively. Similarly, a total of 37 simulations have been conducted by simultaneously adjusting parameters on both surfaces to the same extend as presented above except for the condition of $[SC]_l$ and $[SC]_s$, which adds one more trial (0-fold). Simply diminishing $[SC]_l$ to zero only on luminal face will cause the significant deviation of initial quantitative values for key variables from the equilibrium which ultimately cause the breakdown of the model operation, we thus explore the impact of negative surface charges by concurrently increasing $[SC]_l$ and $[SC]_s$ on both sides. For all of the 0-fold changes related to $[SP]_l/[SP]_s$, K_{cmgl}/K_{cmgs}, K_{pmgl}/K_{pmgs}, K_{pkl}/K_{pks}, and K_{phl}/K_{phs}, the modeled traces rarely show the difference to the standard curves. Therefore, only the controlled traces will be presented in figures. In brief, all simulations (73 trials) that show the obvious alteration compared to the controlled simulation are shown in **Figure 3**. These alterations can basically be summarized into the following three types: (i), the $\Delta\Psi_m$ curve induced by the increased K_{cmgl} was characterized as a more negative starting point, a higher peak, a faster decay till reaching the steady-state during the light phase as well as a more rapid fall followed by an accelerated relaxation in the darkness (**Figure 3A**). This pattern was also reproduced in **Figures 3D,E** *via* 100-fold increasing K_{cmgl} or $[SP]_l$ whereas the variation appears to be less prominent for the change of 10-fold of the controlled value (**Figures 3D,E**). The variation for the $\Delta\Psi_m$ curve was due to an upleveled $\Delta\Psi_d$ (**Figure 4A**) and a crossover of $\Delta\Psi_{dn}$ from the positive to the negative (**Figure 5A**) which is mainly contributed by a less negative Ψ_{dnl} (**Figure 5G**) whereas Ψ_{dns} is slightly affected (**Figure 5D**). (ii), the $\Delta\Psi_m$ curve for the increased $[SC]_l$ (**Figure 3B**) contains the kinetic behavior antiparallel to the curve caused by the increased K_{cmgl}. This was due to a significantly decreased $\Delta\Psi_d$ (**Figure 4B**) and a more positive $\Delta\Psi_{dn}$ (**Figure 5B**) majorly contributed by an enormously negative Ψ_{dnl} (**Figure 5H**); (iii), the $\Delta\Psi_m$ kinetics shows a different pattern induced by concurrently increasing $[SC]_l$ and $[SC]_s$ (**Figure 3C**), which shows a sharp rise as the

light is switched on before experiencing a biphasic decay (a rapid decay followed by a slower decay) till reaching a steady-level. When the light is switched off, the $\Delta\Psi_m$ kinetics shows a sharp fall below the dark baseline before returning to the steady-state much faster than in the controlled trace, whereas a much slower relaxation is visible for 0-fold of the controlled values (**Figure 3C**).

Overall, $\Delta\Psi_{dn}$ and Ψ_{dns} progress in the same trend, i.e., the curve shows a rapid rise as illumination commences before attaining the steady-level followed by an exponential decay till the steady-state is reached as the light is switched off (**Figures 5A–F**). In contrast, the Ψ_{dnl} trace exhibits an opposite behavior which shows a rapid fall before attaining the steady-level followed by a slower rise till relaxing to the steady-state as the light is switched off (**Figures 5G–I**). The $\Delta\Psi_{dn}$ curve was transferred to a more negative level by increasing K_{cmgl} (**Figure 5A**). This was majorly contributed by a smaller Ψ_{dnl} produced (less negative, **Figure 5G**). Intriguingly, increasing K_{cmgl} will cause a slight decrease of Ψ_{dns} (**Figure 5D**) which may be associated with the ion redistribution caused by various ionic fluxes. When increasing $[SC]_l$, the $\Delta\Psi_{dn}$ trace was transferred to a more positive level (**Figure 5B**) due to a much larger Ψ_{dnl} (more negative, **Figure 5H**) together with a slight increase of Ψ_{dns} produced (**Figure 5E**). When concurrently increasing $[SC]_l$ and $[SC]_s$, the $\Delta\Psi_{dn}$ trace was transferred to a much smaller positive level (**Figure 5C**) due to a much larger Ψ_{dnl} (more negative as shown in **Figure 5I** similar as induced by individually increasing $[SC]_l$ in **Figure 5I**) together with a significant upregulation of Ψ_{dns} produced (more negative as shown in **Figure 5F** for Ψ_{dnl}).

When K_{cmgl} or $[SC]_l$ is increased, the $\Delta\Psi_d$ curve is as a whole upshifted to a more positive level (**Figure 4A**) or downshifted to a more negative level (**Figure 4B**) with an extent for the latter is a bit larger than the former. When concurrently increasing $[SC]_l$ and $[SC]_s$, the $\Delta\Psi_d$ curve (**Figure 4C**) decays in a biphasic pattern till saturating in the light phase and shows an accelerated rise returning to the steady-state in the darkness.

When increasing K_{cmgl} 10-fold of the controlled value, the $\Delta\Psi_h$ curve reaches a higher peak ($\sim$70 mV) followed by a more prominent dip as the light is switched on till saturating to a larger steady-level ($\sim$75 mV) (**Figure 2A**). As shutting off the light, the $\Delta\Psi_h$ curve shows a rapid fall followed by an accelerated rise till reaching the steady-state slightly above the dark baseline (**Figure 2A**). The steady-state value of the $\Delta\Psi_k$ curve for 10-fold condition is smaller (less negative) than the standard curve during the light phase (**Figure 2D**) and a more speeded relaxation occurs until reaching the steady-state significantly above the dark baseline as shutting off the light (**Figure 2D**). The steady-state value of the $\Delta\Psi_{cl}$ curve for 10-fold condition is a bit smaller (less negative) than the standard trace during the light phase (**Figure 2G**). As switching off the light, the $\Delta\Psi_{cl}$ curve shows a sharp rise followed by a decelerated exponential decay till reaching

a steady-state moderately above the dark baseline than the controlled curve (**Figure 2G**).

When increasing $[SC]_l$ 10-fold of the controlled value, the $\Delta\Psi_h$ curve peaks at a lower level followed by a nearly diminished dip as switching on the light till saturating to a much smaller steady-level ($\sim$58 mV) (**Figure 2B**). As shutting off the light, the $\Delta\Psi_h$ curve shows a rapid fall followed by a faster rise till reaching the steady-state enormously below the dark baseline (**Figure 2B**). Upon the 10-fold increase of $[SC]_l$, the $\Delta\Psi_k$ curve shows a sharp fall followed by an acute dip till attaining the steady-level much higher (more negative) than the standard trace during the light phase (**Figure 2E**). As shutting off the light, an accelerated relaxation occurs until reaching the steady-state $\sim$10 mV below the dark baseline (**Figure 2E**). Similarly, upon the 10-fold increase of $[SC]_l$, the $\Delta\Psi_{cl}$ curve shows a slower exponential decay till attaining the steady-level much higher (more negative) than the controlled trace during the light phase (more negative, **Figure 2H**). As shutting off the light, the $\Delta\Psi_{cl}$ curve shows a sharp rise reaching a smaller peak level ($\sim$20 mV) followed by a much faster decay till reaching the steady-state $\sim$10 mV below the dark baseline (**Figure 2H**).

When concurrently increasing $[SC]_l$ and $[SC]_s$ 10-fold of the controlled value, the $\Delta\Psi_h$ curve reaches the peak followed by a fast rise to a maximum at $\sim$25 s before decaying to a slightly smaller steady-level ($\sim$62 mV) than the standard curve (**Figure 2C**). As switching off the light, the $\Delta\Psi_h$ curve shows a sharp fall followed by a faster rise till reaching the dark baseline (**Figure 2C**). The $\Delta\Psi_k$ curve upon the 10-fold increase of $[SC]_l$ and $[SC]_s$ shows a sharp fall to about $\sim$35 mV followed by a fast rise till leveling toward a smaller steady-level ($\sim$25 mV) (**Figure 2F**). As switching off the light, a faster relaxation occurs until converging to the dark baseline as the controlled trace (**Figure 2F**). Upon concurrently increasing $[SC]_l$ and $[SC]_s$ 10-fold of the controlled value, the $\Delta\Psi_{cl}$ curve shows a slower exponential decay till attaining the steady-level smaller (less negative) than the controlled curve in the light phase (**Figure 2I**). As switching off the light, the $\Delta\Psi_{cl}$ curve shows a sharp rise peaking at a smaller level ($\sim$25 mV) followed by an accelerated decay till converging to the dark baseline concomitant with the standard trace (**Figure 2I**).

Discussion

Specific roles of ion binding to the membrane-surface on regulating $\Delta\Psi_{dn}$, $\Delta\Psi_d$, and $\Delta\Psi_m$

To investigate specific roles of ion binding to the membrane-surface on regulating $\Delta\Psi_{dn}$, $\Delta\Psi_d$, and $\Delta\Psi_m$, controlling parameters which affect the electric characteristics adjacent to the membrane surface (i.e., K_{cmgl}, K_{cmgs}, K_{pmgl}, K_{pmgs}, K_{pkl}, K_{pks}, K_{phl}, K_{chs}, $[SC]_l$, $[SC]_s$, $[SP]_l$, and $[SP]_s$) were adjusted
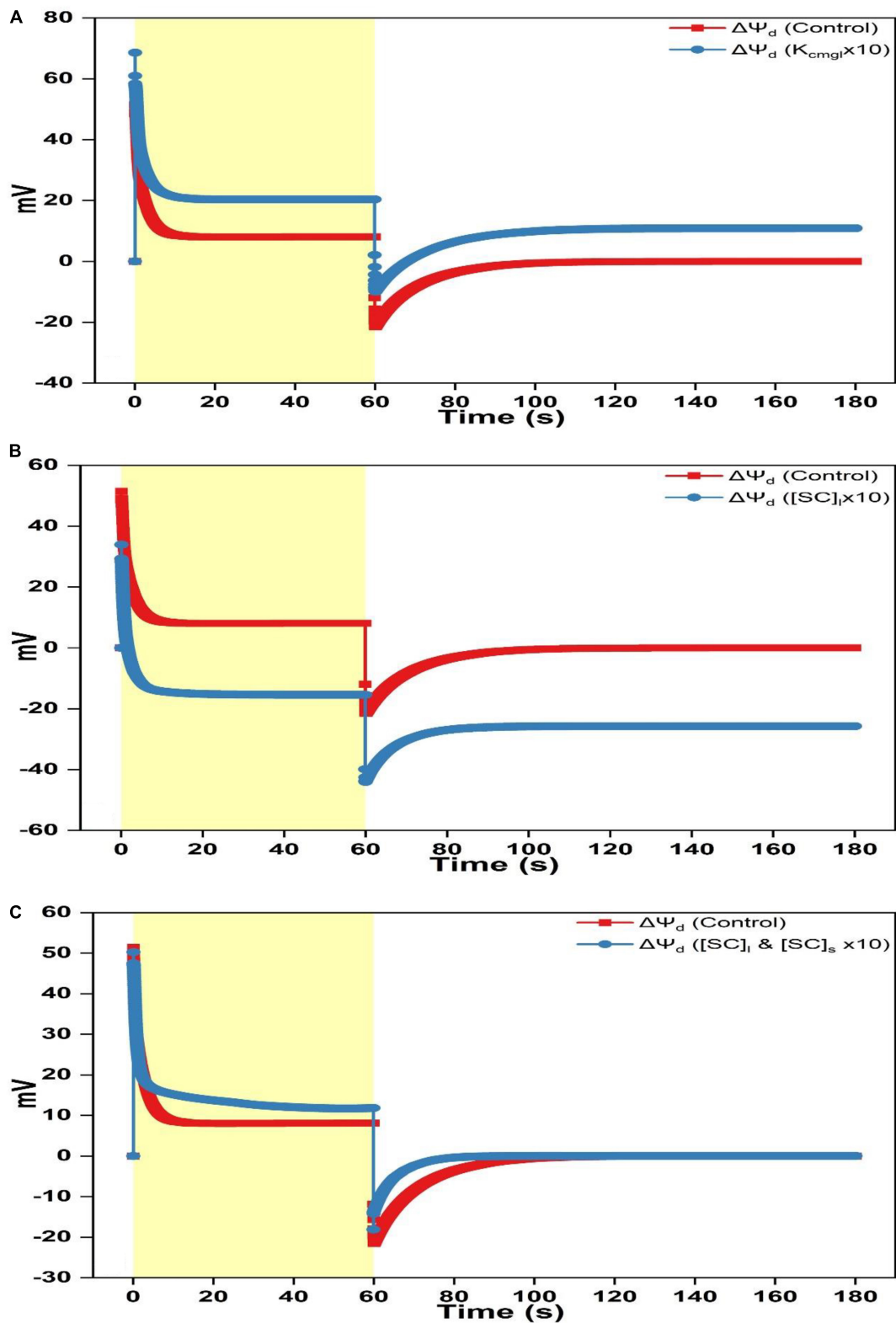
FIGURE 4

Simulated responses of $\Delta\Psi_d$ on assigning different values for adjustable parameters. **(A)** Simulated responses of $\Delta\Psi_d$ by adjusting K_{cmgl} 1- and 10-fold of the controlled value. **(B)** Simulated responses of $\Delta\Psi_d$ by adjusting $[SC]_l$ 1- and 10-fold of the controlled value. **(C)** Simulated responses of $\Delta\Psi_d$ by adjusting $[SC]_l$ and $[SC]_s$ 1- and 10-fold of the controlled value.
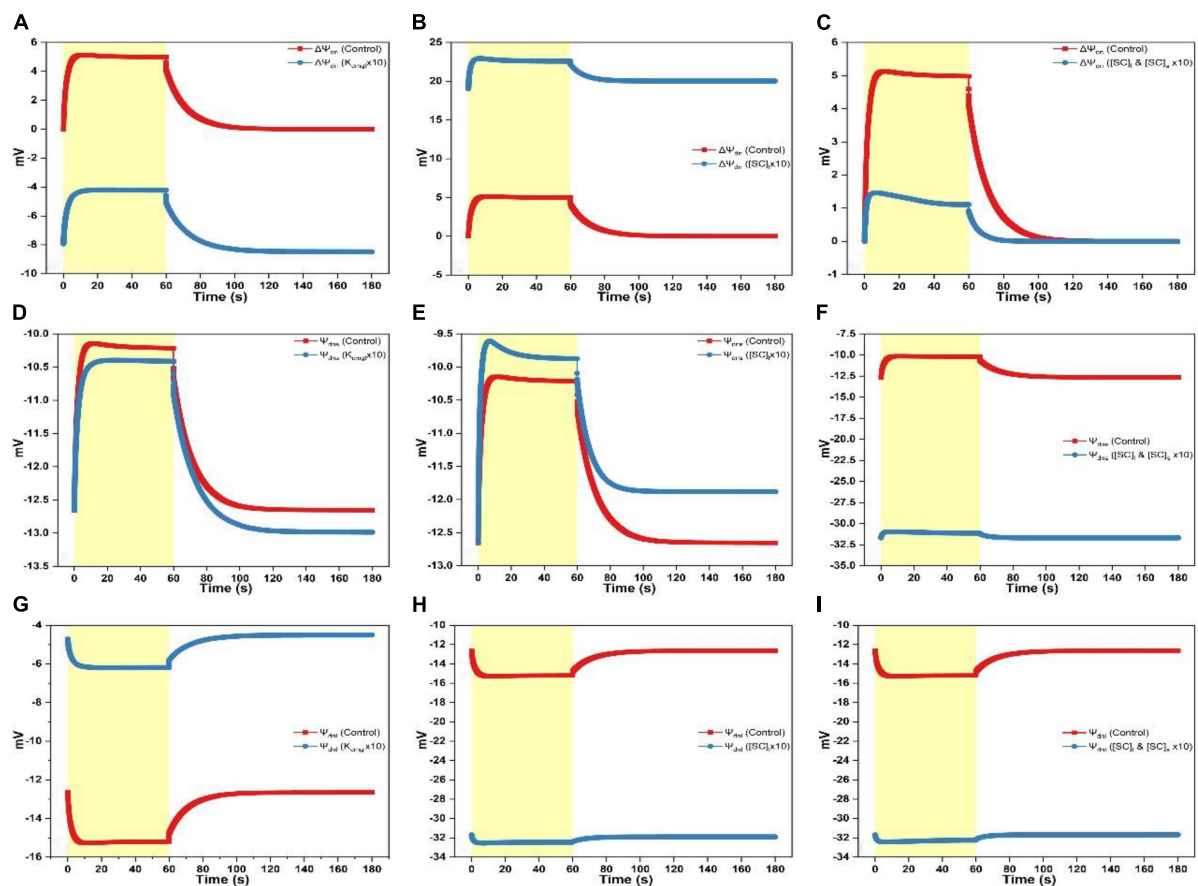
FIGURE 5
Simulated responses of Ψ_{dnl}, Ψ_{dns}, and $\Delta\Psi_{dn}$ on assigning different values for adjustable parameters. **(A)** Simulated responses of $\Delta\Psi_{dn}$ by adjusting K_{cmgl} 1- and 10-fold of the controlled value. **(B)** Simulated responses of $\Delta\Psi_{dn}$ by adjusting $[SC]_l$ 1- and 10-fold of the controlled value. **(C)** Simulated responses of $\Delta\Psi_{dn}$ by adjusting $[SC]_l$ and $[SC]_s$ 1- and 10-fold of the controlled value. **(D)** Simulated responses of Ψ_{dns} by adjusting K_{cmgl} 1- and 10-fold of the controlled value. **(E)** Simulated responses of Ψ_{dns} by adjusting $[SC]_l$ 1- and 10-fold of the controlled value. **(F)** Simulated responses of Ψ_{dns} by adjusting $[SC]_l$ and $[SC]_s$ 1- and 10-fold of the controlled value. **(G)** Simulated responses of Ψ_{dnl} by adjusting K_{cmgl} 1- and 10-fold of the controlled value. **(H)** Simulated responses of Ψ_{dnl} by adjusting $[SC]_l$ 1- and 10-fold of the controlled value. **(I)** Simulated responses of Ψ_{dnl} by adjusting $[SC]_l$ and $[SC]_s$ 1- and 10-fold of the controlled value.

under various scenarios to conduct *in silico* experiments. Computing findings reveal that approximate three types of variations induced by the adjustable parameters may be derived as follows: (i) The K_{cmgl}-induced type, (ii) the $[SC]_l$-induced type, and (iii) the $[SC]_l$ and $[SC]_s$-induced type. For the K_{cmgl}-induced type, high binding constant for Mg^{2+} reduces the negativity of Ψ_{dnl} (**Figure 5G**), which increases the concentration of Cl^- while decreases the concentration of cations (K^+ and H^+) close to the membrane-surface. This causes a larger Cl^- flux penetrating the membrane (**Supplementary Figure 2B**) and a larger concentration of H^+ kept in the bulk phase (**Supplementary Figure 3B**). However, a more significant K^+ flux cannot be notably observed (**Supplementary Figure 1B**). The K_{cmgl}-induced ion flux mediated by the KEA3 is slightly smaller than the controlled (**Supplementary Figure 1D**). The KEA3 functions to maintain the level of $\Delta\Psi_m$ while decreasing the pH in lumen through

the exchange of cations between K^+ (in) and H^+ (out) (Kunz et al., 2014; Armbruster et al., 2016; Wang et al., 2017; Wang and Shikanai, 2019). Additionally, the effect of ion flux mediated by the Cl^- channel CLCe is trivial ($\sim10^{-4}$ mM/s) (**Supplementary Figure 2D**). This result was also visible in the computing data from Li et al. (2021). Conceivably, more Cl^- traveling to the stroma will increase the negativity of Ψ_{dns} (**Figure 5D**), in addition to the less negative Ψ_{dnl}, which ultimately converts the total Donnan potential ($\Delta\Psi_{dn}$) to negative values (**Figure 5A**). This, in turn, keeps the steady-level of $\Delta\Psi_m$ only marginally altered by playing an essential counterpart against the highly increased $\Delta\Psi_d$ (**Figure 4A**) due to the co-function of $\Delta\Psi_h$ (**Figure 2A**), $\Delta\Psi_k$ (**Figure 2D**), and $\Delta\Psi_{cl}$ (**Figure 2G**). It should also be noted that the kinetics of $\Delta\Psi_{dn}$, $\Delta\Psi_d$, and $\Delta\Psi_m$ as the light is switched off relaxes in the same pattern as described above. This holds in all simulations for three patterns.

For the $[SC]_l$-induced type, the consequence is, in fact, antiparallel to those induced by the high binding constant for Mg^{2+}, since high abundance of negative charge sites increases the negativity of Ψ_{dnl} (**Figure 5H**), which in turn increases the concentration of cations (K^+ and H^+) while decreasing the concentration of Cl^- close to the membrane-surface. This causes a larger transmembrane K^+ flux (**Supplementary Figure 1B**) and a smaller concentration of H^+ stored in the bulk-phase (**Supplementary Figure 3B**) whereas a significantly reduced Cl^- flux cannot be notably observed (**Supplementary Figure 2B**). This might imply that the Cl^- enrichment close to the membrane-surface is likely to be more affected by the "screening" effect caused by cations binding to the surface charges nor the abundance of negative charge sites themselves. Understandably, more K^+ traveling to the stroma will decreases the negativity of Ψ_{dns} (**Figure 5E**), in addition to the more negative Ψ_{dnl}, which ultimately produce a more positive value for the Donnan potential ($\Delta\Psi_{dn}$) (**Figure 5B**). However, under this condition, the co-function of $\Delta\Psi_h$ (**Figure 2B**), $\Delta\Psi_k$ (**Figure 2E**), and $\Delta\Psi_{cl}$ (**Figure 2H**) makes $\Delta\Psi_d$ a value being enormously negative (**Figure 4B**), which eventually decreases the steady-level of $\Delta\Psi_m$ (**Figure 3B**) with an extent a bit larger than in the K_{cmgl}-induced type (**Figure 3A**). This might demonstrate that, by identically enlarging K_{cmgl} or $[SC]_l$ 10-fold of the controlled, the abundance of the negative charge sites will cause more pronounced effects on regulating $\Delta\Psi_{dn}$, $\Delta\Psi_d$, and $\Delta\Psi_m$ than the K_{cmgl}-induced type.

When concurrently increasing $[SC]_l$ and $[SC]_s$, i.e., for the $[SC]_l$ and $[SC]_s$-induced type, the high abundance of negative charge sites on both surfaces can concomitantly reduce both the negativity of Ψ_{dnl} and Ψ_{dns} (**Figures 5F,I**). This triggers the kinetic behavior a complexity compared to the K_{cmgl}-induced or the $[SC]_l$-induced type. With the negativity decrease for Ψ_{dnl} and Ψ_{dns}, the Cl^- flux density is largely reduced (**Supplementary Figure 2B**) but the enormously increased H^+ (out)/K^+ (in) flux conducted by the KEA3 (**Supplementary Figure 1D**) is observed following a complex dynamic pattern (a sharp rise followed by a deep well till leveling off) as the light is switched on. Intriguingly, the K^+ flux nearly remains unaffected (**Supplementary Figure 1B**). The resultant effect of all ion fluxes causes a positive $\Delta\Psi_{dn}$ with a small amplitude (**Figure 5C**) and makes the steady-state $\Delta\Psi_d$ reach a value being more positive (**Figure 4C**). However, it is unparallel to the standard curve but softly decaying till saturating. Similarly, the $\Delta\Psi_m$ bears a resemblance to $\Delta\Psi_d$ but being more positive because it is apparent that the addition of $\Delta\Psi_d$ and $\Delta\Psi_{dn}$ (being positive) produces the $\Delta\Psi_m$. Taken together, our simulations show that Ψ_{dn} can affect the concentration of ions close to the membrane-surface and thus the diffuse potential ($\Delta\Psi_d$) and consequently the total membrane potential ($\Delta\Psi_m$). Therefore, Ψ_{dn} plays a key role on regulating the thylakoid-membrane energization during photosynthesis and should be considered

in future studies, which are related to the transthylakoid electrical potential.

Role of a Mg^{2+} flux through the thylakoid membrane

As noted, thylakoid-harbored non-selective cation pores are not only permeable to K^+ but also to Mg^{2+} (Enz et al., 1993; Pottosin and Schönknecht, 1996), causing a rise, upon illumination, of Mg^{2+} concentration in the stroma by 1–5 mM (Krause, 1977; Portis, 1981). To check the role of Mg^{2+} on regulating $\Delta\Psi_m$, we additionally merged a Mg^{2+} flux calculated by the GHK equation similar to K^+ flux into our model and the value of permeability for Mg^{2+} was set at one-third of that for K^+ based on the measuring data from Pottosin and Schönknecht (1996), i.e., the single channel conductance is 60 pS for K^+ and 19 pS for Mg^{2+}. It turns out that, although several local features of the $\Delta\Psi_m$ (the total membrane potential) trace were altered (data not shown), the general kinetic trend keeps unaffected, which also shows a sharp rise upon illumination before decaying to certain extent of its initial amplitude and then rising again till reaching a steady-state. When the light is switched off, the $\Delta\Psi_m$ curve also shows a sharp fall before returning to the dark baseline. The unaffected kinetic trend might be explained by the fact that more cationic effluxes into stroma would cause a raised dissipation for the diffusion potential difference ($\Delta\Psi_d$). On the other hand, more cations entry into stroma would cause an increase for the negativity of Ψ_{dnl} but a concomitant decrease for the negativity of Ψ_{dns}, ultimately triggering a rise of the Donnan potential difference ($\Delta\Psi_{dn}$), which compensates the loss of $\Delta\Psi_d$. Furthermore, we also conducted the simulations under which principles for regulations by the altered parameters on $\Delta\Psi_m$ remain unchanged as those shown in **Figure 3**. For instance, the $\Delta\Psi_m$ curve induced by the increased K_{cmgl} (control, ×5, and ×10) was also characterized as a more negative starting point, a higher peak, a faster decay till reaching the steady-state during the light phase as well as a more rapid fall followed by an accelerated relaxation returning to the baseline in the darkness. In essence, the adjustment of $\Delta\Psi_m$ by the Mg^{2+} efflux manifests an "identical" effect as by the K^+ efflux because they both are cations and merely differ in their valences.

Donnan potential or surface potential at the thylakoid membrane?

It has been shown that both surfaces of the thylakoid membrane carry fixed negative charges (Barber, 1980b, 1982).

An electrical potential difference is thus established between the membrane surface and the electrolyte solution, which is sufficiently negative to enrich the concentration of cations or to deplete the concentration of anions close to the thylakoid membrane surface. This electric potential has been mathematically computed by two different approaches, i.e., the Donnan equilibrium potential or the Gouy–Chapman double-layer potential (the surface potential is termed as a synonym). As noted above, the surface potential assumes that the thickness of membrane surface charge layer (d_s) is zero and all membrane fixed charges are only located within the membrane surface. Theoretically, provided $d_s \geq 1/\kappa$ (κ being the Debye–Hückel parameter), the electric potential in the region far inside the charge layer is practically equal to the Donnan potential (Ohshima and Ohki, 1985; Ohshima and Kondo, 1988b, 1990). Provided $d_s \leq 1/\kappa$, the electric potential at the membrane surface is practically equal to the surface potential. The Donnan potential ($d_s \rightarrow \infty$) can be converted to the surface potential ($d_s \rightarrow 0$) undergoing a smooth transition (Ohshima and Kondo, 1990). In essence, the surface potential is a transformer of the Donnan potential as d_s is approaching zero (Ohshima and Kondo, 1990). Up to the present, all attempts to estimate d_s have been subject to artifacts (Levine et al., 1983). Additionally, using the initial values of our model for all solute species, $1/\kappa$ for the thylakoid membrane is calculated as 61.5 nm (see **Supplementary Material**). Although the characterization of electric potential is dependent on d_s, it is still adequate to assume the inner space of the chloroplast as a Donnan system because the Gouy–Chapman potential is essentially an alternative "Donnan potential" at the extrema. Additionally, the Donnan potential has particularly been appropriate for studies of ion transport processes through membrane (Ohshima and Ohki, 1985). In our study, at the standard state, the Donnan potential is computed as within ~ -12.5 to ~ -10 mV for the luminal compartment (Ψ_{dnl}) (**Figure 1C**) and ~ -15 to ~ -12.5 mV for the stromal compartment (Ψ_{dns}) (**Figure 1C**), both of which agree with the literature data (Sperelakis, 2012; Qasem et al., 2018).

Conclusion

By employing an extended photosynthetic model, we investigated the effect of altered cationic binding to the negatively charged thylakoid membrane surface on adjusting the transthylakoid electric potential focusing on a cycle of illumination followed by a dark-adapted period. Consequently, the measured ECS traces were well described by the computing results by assigning the model parameters with the quantitative values taken from the literature. Moreover, the computing data clarified the components of transthylakoid membrane potential, unraveled the functional consequences of altered cationic attachment to the membrane surface on adjusting

the transthylakoid electric potential, and revealed the key role played by the Donnan potential in bridging the diffusion potential with the total membrane potential. Ultimately, the compatibility of Donnan theory employed in the chloroplast in conjunction with the interrelationship between the Donnan potential and the Gouy–Chapman potential were discussed. The current model presented in this work can serve as a basis for further extension into a more detailed theoretical model by which multiple variables involved in photosynthesis can be explored.

Data availability statement

The original contributions presented in this study are included in the article/**Supplementary Material**, further inquiries can be directed to the corresponding authors.

Author contributions

HL conceived the study, performed the experiments, constructed the model, performed the simulations, and wrote parts of the manuscript. DL analyzed the experimental data, constructed the model, wrote parts of the manuscript, and supervised the referencing. Both authors contributed to the article and approved the submitted version.

Funding

Acknowledgments

Conflict of interest

The authors declare that the research was conducted in the absence of any commercial or financial relationships that could be construed as a potential conflict of interest.

Publisher's note

All claims expressed in this article are solely those of the authors and do not necessarily represent those of their affiliated organizations, or those of the publisher, the editors and the reviewers. Any product that may be evaluated in this article, or claim that may be made by its manufacturer, is not guaranteed or endorsed by the publisher.

Supplementary material

The Supplementary Material for this article can be found online at: https://www.frontiersin.org/articles/10.3389/fpls.2022.945675/full#supplementary-material

SUPPLEMENTARY FIGURE 1
Simulated responses of the K^+ flux and the H^+/K^+ flux on assigning different values for adjustable parameters. **(A)** 3D view of the K^+-flux kinetics simulated under control and by 10-fold increasing K_{cmgl}, $[SC]_l$, and $[SC]_l$ and $[SC]_s$, respectively; **(B)** 2D view of the K^+-flux kinetics simulated under control and by 10-fold increasing K_{cmgl}, $[SC]_l$, and $[SC]_l$ and $[SC]_s$, respectively; **(C)** 3D view of the H^+/K^+-flux kinetics simulated under control and by 10-fold increasing K_{cmgl}, $[SC]_l$, and $[SC]_l$ and $[SC]_s$, respectively; **(D)** 2D view of the H^+/K^+-flux kinetics simulated under control and by 10-fold increasing K_{cmgl}, $[SC]_l$, and $[SC]_l$ and $[SC]_s$, respectively.

SUPPLEMENTARY FIGURE 2
Simulated responses of the Cl^- flux and the H^+/Cl^- flux on assigning different values for adjustable parameters. **(A)** 3D view of the Cl^--flux kinetics simulated under control and by 10-fold increasing K_{cmgl}, $[SC]_l$, and $[SC]_l$ and $[SC]_s$, respectively; **(B)** 2D view of the Cl^--flux kinetics simulated under control and by 10-fold increasing K_{cmgl}, $[SC]_l$, and $[SC]_l$ and $[SC]_s$, respectively; **(C)** 3D view of the H^+/Cl^--flux kinetics simulated under control and by 10-fold increasing K_{cmgl}, $[SC]_l$, and $[SC]_l$ and $[SC]_s$, respectively; **(D)** 2D view of the H^+/Cl^--flux kinetics simulated under control and by 10-fold increasing K_{cmgl}, $[SC]_l$, and $[SC]_l$ and $[SC]_s$, respectively.

SUPPLEMENTARY FIGURE 3
Simulated responses of $[H^+]_l$ and $[H^+]_s$ on assigning different values for adjustable parameters. **(A)** 3D view of $[H^+]_l$ responses simulated under control and by 10-fold increasing K_{cmgl}, $[SC]_l$, and $[SC]_l$ and $[SC]_s$, respectively; **(B)** 2D view of the $[H^+]_l$ responses simulated under control and by 10-fold increasing K_{cmgl}, $[SC]_l$, and $[SC]_l$ and $[SC]_s$, respectively; **(C)** 3D view of the $[H^+]_s$ responses simulated under control and by 10-fold increasing K_{cmgl}, $[SC]_l$, and $[SC]_l$ and $[SC]_s$, respectively; **(D)** 2D view of the $[H^+]_s$ responses simulated under control and by 10-fold increasing K_{cmgl}, $[SC]_l$, and $[SC]_l$ and $[SC]_s$, respectively.

References

Armbruster, U., Leonelli, L., Correa Galvis, V., Strand, D., Quinn, E. H., Jonikas, M. C., et al. (2016). Regulation and Levels of the Thylakoid K+/H+ Antiporter KEA3 Shape the dynamic response of photosynthesis in fluctuating light. *Plant Cell Physiol.* 57, 1557–1567. doi: 10.1093/pcp/pcw085

Barber, J. (1980b). Membrane surface charges and potentials in relation to photosynthesis. *Biochim. Biophys. Acta* 594, 253–308.

Barber, J. (1980a). An explanation for the relationship between salt-induced thylakoid stacking and the chlorophyll fluorescence changes associated with changes in spillover of energy from photosystem II to photosystem I. *FEBS Lett.* 118, 1–10.

Barber, J. (1982). Influence of surface charges on thylakoid structure and function. *Annu. Rev. Plant Physiol.* 33, 261–295.

Barber, J., Mills, J., and Love, A. (1977). Electrical diffuse layers and their influence on photosynthetic processes. *FEBS Lett.* 74, 174–181.

Basso, L., Yamori, W., Szabo, I., and Shikanai, T. (2020). Collaboration between NDH and KEA3 allows maximally efficient photosynthesis after a long dark adaptation. *Plant Physiol.* 184, 2078–2090. doi: 10.1104/pp.20.01069

Bulychev, A. A. (1984). Different kinetics of membrane potential formation in dark-adapted and preilluminated chloroplasts. *Biochim. Biophys. Acta* 766, 647–652. doi: 10.1007/s10863-012-9476-6

Bulychev, A. A., and Vredenberg, W. J. (1999). Light-triggered electrical events in the thylakoid membrane of plant chloroplasts. *Physiol. Plant.* 105, 577–584.

Correa Galvis, V., Strand, D. D., Messer, M., Thiele, W., Bethmann, S., Hubner, D., et al. (2020). H(+) Transport by K(+) EXCHANGE ANTIPORTER3 Promotes Photosynthesis and Growth in Chloroplast ATP Synthase Mutants. *Plant Physiol.* 182, 2126–2142. doi: 10.1104/pp.19.01561

Cruz, J. A., Kanazawa, A., Treff, N., and Kramer, D. M. (2005). Storage of light-driven transthylakoid proton motive force as an electric field (Deltapsi) under steady-state conditions in intact cells of *Chlamydomonas reinhardtii*. *Photosynth. Res.* 85, 221–233. doi: 10.1007/s11120-005-4731-x

Cruz, J. A., Sacksteder, C. A., Kanazawa, A., and Kramer, D. M. (2001). Contribution of electric field (Delta psi) to steady-state transthylakoid proton motive force (pmf) *in vitro* and *in vivo*. control of pmf parsing into Delta psi and Delta pH by ionic strength. *Biochemistry* 40, 1226–1237. doi: 10.1021/bi0018741

Davis, G. A., Kanazawa, A., Schottler, M. A., Kohzuma, K., Froehlich, J. E., Rutherford, A. W., et al. (2016). Limitations to photosynthesis by proton motive

force-induced photosystem II photodamage. *eLife* 5:e16921. doi: 10.7554/eLife.16921

Davis, G. A., Rutherford, A. W., and Kramer, D. M. (2017). Hacking the thylakoid proton motive force for improved photosynthesis: modulating ion flux rates that control proton motive force partitioning into Deltapsi and DeltapH. *Philos. Trans. R. Soc. Lond. B Biol. Sci.* 372:20160381. doi: 10.1098/rstb.2016.0381

Enz, C., Steinkamp, T., and Wagner, R. (1993). Ion channels in the thylakoid membrane (A patch-clamp study). *Biochim. Biophys. Acta* 1143, 67–76. doi: 10.1016/0005-2728(93)90217-4

Gillespie, D., and Eisenberg, R. S. (2001). Modified Donnan potentials for ion transport through biological ion channels. *Phys. Rev. E Stat. Nonlin. Soft. Matter. Phys.* 63:061902.

Herdean, A., Teardo, E., Nilsson, A. K., Pfeil, B. E., Johansson, O. N., Unnep, R., et al. (2016b). A voltage-dependent chloride channel fine-tunes photosynthesis in plants. *Nat. Commun.* 7:11654. doi: 10.1038/ncomms11654

Herdean, A., Nziengui, H., Zsiros, O., Solymosi, K., Garab, G., Lundin, B., et al. (2016a). The Arabidopsis Thylakoid Chloride Channel AtCLCe functions in chloride homeostasis and regulation of photosynthetic electron transport. *Front. Plant Sci.* 7:115. doi: 10.3389/fpls.2016.00115

Johnson, M. P., and Ruban, A. V. (2014). Rethinking the existence of a steady-state Deltapsi component of the proton motive force across plant thylakoid membranes. *Photosynth. Res.* 119, 233–242. doi: 10.1007/s11120-013-9817-2

Joliot, P., and Joliot, A. (1989). Characterization of linear and quadratic electrochromic probes in *Chlorella sorokiniana* and *Chlamydomonas reinhardtii*. *Biochim. Biophys. Acta* 975, 355–360.

Kaňa, R., and Govindjee. (2016). Role of ions in the regulation of light-harvesting. *Front. Plant Sci.* 7:1849. doi: 10.3389/fpls.2016.01849

Kanazawa, A., Ostendorf, E., Kohzuma, K., Hoh, D., Strand, D. D., Sato-Cruz, M., et al. (2017). Chloroplast ATP synthase modulation of the thylakoid proton motive force: implications for Photosystem I and Photosystem II Photoprotection. *Front. Plant Sci.* 8:719. doi: 10.3389/fpls.2017.00719

Kinraide, T. B., Yermiyahu, U., and Rytwo, G. (1998). Computation of surface electrical potentials of plant cell membranes. Correspondence To published zeta potentials from diverse plant sources. *Plant Physiol.* 118, 505–512. doi: 10.1104/pp.118.2.505

Klughammer, C., Siebke, K., and Schreiber, U. (2013). Continuous ECS-indicated recording of the proton-motive charge flux in leaves. *Photosynth. Res.* 117, 471–487. doi: 10.1007/s11120-013-9884-4

Kramer, D. M., and Sacksteder, C. A. (1998). A diffused-optics flash kinetic spectrophotometer (DOFS) for measurements of absorbance changes in intact plants in the steady-state. *Photosynth. Res.* 56, 103–112.

Kramer, D. M., Sacksteder, C. A., and Cruz, J. A. (1999). How acidic is the lumen? *Photosynth. Res.* 60, 151–163.

Krause, G.H. (1977). Light-induced movement of magnesium ions in intact chloroplasts. Spectroscopic determination with Eriochrome Blue SE. *Biochim. Biophys. Acta.* 460, 500–510.

Kunz, H. H., Gierth, M., Herdean, A., Satoh-Cruz, M., Kramer, D. M., Spetea, C., et al. (2014). Plastidial transporters KEA1, -2, and -3 are essential for chloroplast osmoregulation, integrity, and pH regulation in Arabidopsis. *Proc. Natl. Acad. Sci. U.S.A.* 111, 7480–7485. doi: 10.1073/pnas.1323899111

Levine, S., Levine, M., Sharp, K. A., and Brooks, D. E. (1983). Theory of the electrokinetic behavior of human erythrocytes. *Biophys. J.* 42, 127–135. doi: 10.1016/S0006-3495(83)84378-1

Li, M., Svoboda, V., Davis, G., Kramer, D., Kunz, H. H., and Kirchhoff, H. (2021). Impact of ion fluxes across thylakoid membranes on photosynthetic electron transport and photoprotection. *Nat. Plants* 7, 979–988. doi: 10.1038/s41477-021-00947-5

Li, Z., Wakao, S., Fischer, B. B., and Niyogi, K. K. (2009). Sensing and responding to excess light. *Annu. Rev. Plant Biol.* 60, 239–260.

Lyu, H., and Lazar, D. (2017a). Modeling the light-induced electric potential difference (DeltaPsi), the pH difference (DeltapH) and the proton motive force across the thylakoid membrane in C3 leaves. *J. Theor. Biol.* 413, 11–23. doi: 10.1016/j.jtbi.2016.10.017

Lyu, H., and Lazar, D. (2017b). Modeling the light-induced electric potential difference DeltaPsi across the thylakoid membrane based on the transition state rate theory. *Biochim. Biophys. Acta Bioenerg.* 1858, 239–248. doi: 10.1016/j.bbabio.2016.12.009

Mitchell, P. (1961). Chemiosmotic coupling in oxidative and photosynthetic phosphorylation. *Biochem. J.* 79, 1507–1538.

Mitchell, P. (1966). Chemiosmotic coupling in oxidative and photosynthetic phosphorylation. *Biol. Rev. Camb. Philos. Soc.* 41, 445–502.

Mitchell, P. (2011). Chemiosmotic coupling in oxidative and photosynthetic phosphorylation. 1966. *Biochim. Biophys. Acta* 1807, 1507–1538.

Nakatani, H. Y., Barber, J., and Forrester, J. A. (1978). Surface charges on chloroplast membranes as studied by particle electrophoresis. *Biochim. Biophys. Acta Bioenerg.* 504, 215–225. doi: 10.1016/0005-2728(78)90019-1

Ohshima, H., and Kondo, T. (1987). Electrostatic repulsion of ion penetrable charged membranes: role of Donnan potential. *J. Theor. Biol.* 128, 187–194. doi: 10.1016/s0022-5193(87)80168-6

Ohshima, H., and Kondo, T. (1988b). Membrane potential and Donnan potential. *Biophys. Chem.* 29, 277–281.

Ohshima, H., and Kondo, T. (1988a). Double-layer interaction regulated by the donnan potential. *J. Colloid Interface Sci.* 123, 136–142. doi: 10.1016/0301-4622(91)85031-k

Ohshima, H., and Kondo, T. (1990). Relationship among the surface potential, Donnan potential and charge density of ion-penetrable

membranes. *Biophys. Chem.* 38, 117–122. doi: 10.1016/0301-4622(90)80046-a

Ohshima, H., and Ohki, S. (1985). Donnan potential and surface potential of a charged membrane. *Biophys. J.* 47, 673–678.

Pinnola, A., and Bassi, R. (2018). Molecular mechanisms involved in plant photoprotection. *Biochem. Soc. Trans.* 46, 467–482.

Portis, A. R. (1981). Evidence of a low stromal Mg2+ concentration in intact chloroplasts in the dark: I. STUDIES WITH THE IONOPHORE A23187. *Plant Physiol.* 67, 985–989

Pottosin, I., and Schönknecht, G. (1996). Ion channel permeable for divalent and monovalent cations in native spinach thylakoid membranes. *J. Membr. Biol.* 152, 223–233. doi: 10.1007/s002329900100

Qasem, N. A. A., Qureshi, B. A., and Zubair, S. M. (2018). Improvement in design of electrodialysis desalination plants by considering the Donnan potential. *Desalination* 441, 62–76.

Schönknecht, G., Hedrich, R., Junge, W., and Raschke, K. (1988). A voltage-dependent chloride channel in the photosynthetic membrane of a higher plant. *Nature* 336, 589–592.

Siggel, U. (1981a). 414 — Surface and/or Donnan potentials at the thylakoid membrane? *Bioelectrochem. Bioenerg.* 8, 327–337.

Siggel, U. (1981b). 415 - Surface and/or Donnan potentials at the thylakoid membrane? *Bioelectrochem. Bioenerg.* 8, 339–346.

Siggel, U. (1981c). 416 - Surface and/or Donnan potentials at the thylakoid membrane? *Bioelectrochem. Bioenerg.* 8, 347–354.

Sperelakis, N. (ed.) (2012). "Gibbs–Donnan Equilibrium Potentials," in *Cell Physiology Source Book*, (San Diego, CA: Academic Press Inc), 147–151.

Tester, M., and Blatt, M.R. (1989). Direct measurement of k channels in thylakoid membranes by incorporation of vesicles into planar lipid bilayers. *Plant Physiol.* 91, 249–252.

Van Kooten, O., Snel, J. F., and Vredenberg, W. J. (1986). Photosynthetic free energy transduction related to the electric potential changes across the thylakoid membrane. *Photosynth. Res.* 9, 211–227. doi: 10.1007/BF00029745

Vredenberg, W. J. (1981). P515: a monitor of photosynthetic energization in chloroplast membranes. *Physiol. Plant.* 53, 598–602.

Vredenberg, W. J. (1997). Electrogenesis in the photosynthetic membrane: fields, facts and features. *Bioelectrochem. Bioenerg.* 44, 1–11.

Vredenberg, W. J., and Bulychev, A. (2003). Photoelectric effects on chlorophyll fluorescence of photosystem II in vivo. Kinetics in the absence and presence of valinomycin. *Bioelectrochemistry* 60, 87–95. doi: 10.1016/s1567-5394(03)00053-7

Wang, C., and Shikanai, T. (2019). Modification of Activity of the Thylakoid H(+)/K(+) Antiporter KEA3 Disturbs pH-Dependent Regulation of Photosynthesis. *Plant Physiol.* 181, 762–773. doi: 10.1104/pp.19.00766

Wang, C., Yamamoto, H., Narumiya, F., Munekage, Y. N., Finazzi, G., Szabo, I., et al. (2017). Fine-tuned regulation of the K(+) /H(+) antiporter KEA3 is required to optimize photosynthesis during induction. *Plant J.* 89, 540–553. doi: 10.1111/tpj.13405

Witt, H. T. (1979). Energy conversion in the functional membrane of photosynthesis. Analysis by light pulse and electric pulse methods. The central role of the electric field. *Biochim. Biophys. Acta* 505, 355–427. doi: 10.1016/0304-4173(79)90008-9